Available online at www.sciencedirect.com
SCIENCE DIRECT®
Engineering Fracture Mechanics 72 (2005) 2647–2671
Engineering Fracture Mechanics
www.elsevier.com/locate/engfracmech

Stress intensity factor equations for branched crack growth

M.A. Meggiolaro [a,*], A.C.O. Miranda [b], J.T.P. Castro [a], L.F. Martha [c]

[a] *Mechanical Engineering Department, Pontifical Catholic University of Rio de Janeiro (PUC-Rio), Rua Marquês de São Vicente 225, Rio de Janeiro, RJ 22453-900, Brazil*
[b] *Tecgraf—Computer Graphics Technology Group, Pontifical Catholic University of Rio de Janeiro (PUC-Rio), Rua Marquês de São Vicente 225, Rio de Janeiro, RJ 22453-900, Brazil*
[c] *Civil Engineering Department, Pontifical Catholic University of Rio de Janeiro (PUC-Rio), Rua Marquês de São Vicente 225, Rio de Janeiro, RJ 22453-900, Brazil*

Received 18 June 2004; received in revised form 12 May 2005; accepted 22 May 2005
Available online 28 July 2005

Abstract

Overload-induced fatigue crack branching is a well-known crack growth retardation or arrest mechanism, which can quantitatively explain such effects even when arguments based on plasticity induced crack closure cannot be applied, e.g. in high *R*-ratio or in plane strain controlled fatigue crack growth. However, the few results available for branched cracks cannot be used to predict the subsequent crack growth nor account for the delays observed in practice. In this work, specialized finite element (FE) and fatigue life assessment software are used to solve this problem. The crack path and associated stress intensity factors (SIF) of kinked and bifurcated cracks are numerically obtained by the FE program for several angles and branch lengths, and the companion life assessment program is used to estimate the number of delay cycles associated with them. From these results, crack retardation equations are proposed to model the number of delay cycles and the retardation factor along the crack path, allowing for a better understanding of the influence of crack deflection in the propagation life of structural components.

Keywords: Crack bifurcation; Crack growth retardation; Finite elements

1. Introduction

It is well known that fatigue cracks can significantly deviate from their Mode I growth direction, generating crack kinking or branching [1] as illustrated in Fig. 1, due to the influence of overloads, multi-axial

* Corresponding author. Tel.: +55 21 3114 1638; fax: +55 21 3114 1165.
E-mail address: meggi@mec.puc-rio.br (M.A. Meggiolaro).

0013-7944/$ - see front matter © 2005 Elsevier Ltd. All rights reserved.
doi:10.1016/j.engfracmech.2005.05.004

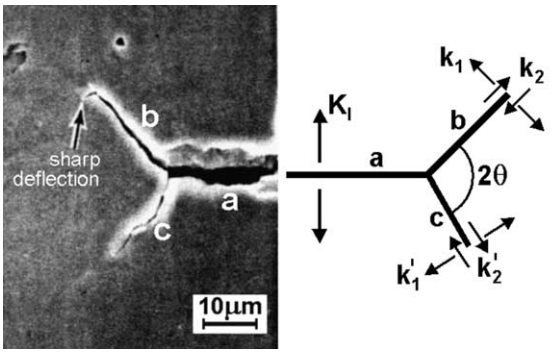

Fig. 1. Bifurcated crack geometry and nomenclature [1].

stresses, microstructural inhomogeneities such as grain boundaries and interfaces, or environmental effects. A fatigue crack deviated from its nominal Mode I plane induces mixed-mode near-tip conditions even if the far-field stress is purely Mode I. For instance, as shown in Fig. 1, a pure Mode I stress intensity factor (SIF) K_I induces Modes I and II SIF k_1 and k_2 near the longer branch of a bifurcated crack and k'_1 and k'_2 near the shorter one. Since these SIF associated to deflected or branched fatigue cracks can be considerably smaller than the SIF of a straight crack with the same projected length, such deviations can retard or even arrest the subsequent crack growth [2]. In addition, the fracture surface roughness generated by such deviations can also alter the crack closure level, leading to further perturbations on the crack propagation rates.

It is experimentally observed that very small differences between the crack branch lengths b and c are enough to cause the shorter branch to arrest as the larger one propagates, generally changing its curvature until reaching approximately its pre-overload SIF and growth direction and rate. Therefore, although many branches can be developed along the main crack path, only the fastest one continues to grow, while all others are brought to a stop due to its shielding effect. This typical propagation behavior has been observed in many structural components, e.g. on a branched crack on an aircraft wheel rim made of 2014-T6 aluminum alloy [3].

Analytical and approximate solutions have been obtained for the SIF of kinked and branched cracks, but it is generally recognized that it is very difficult to develop accurate analytical solutions to their complex propagation behavior [2,4–7]. Presently, therefore, numerical methods such as finite elements (FE) and boundary elements (BE) seem to be the only practical means to predict the propagation behavior of branched cracks. A summary of such SIF solutions as a function of the deflection angle and the length of the deflected part of the crack are presented in [8].

To predict the (generally curved) path of a branched crack and to calculate the associated Modes I and II SIF, a specially developed interactive FE program named Quebra2D (meaning 2D Fracture in Portuguese) is used [9]. This program simulates two-dimensional fracture processes based on a FE self-adaptive strategy, using appropriate crack tip elements and crack increment criteria. The adaptive FE analyses are coupled with modern and very efficient automatic remeshing schemes. The remeshing algorithm developed for Quebra2D works both for regions without cracks and for regions with one or multiple cracks, which may be either embedded or surface breaking. Moreover, this algorithm is numerically stable even when the ratio between the largest and the smallest FE is higher than 10^3. The program is validated through experiments on ESE(T) and modified C(T) specimens made of 4340 and 1020 steel, and from comparisons with analytical solutions.

The crack path and its associated SIF are then exported to ViDa, a general-purpose fatigue design program developed to predict both initiation and propagation fatigue lives under variable loading by all classical design methods [10]. It includes comprehensive databases of stress concentration and intensity factors,

crack propagation models and material properties, rain-flow counters, graphical output for all computed results, including elastic–plastic hysteresis loops and 2D crack fronts. In particular, its crack propagation module accepts any stress-intensity factor expression, including the ones generated by FE software. In this way, ViDa works as a companion life assessment program to the Quebra2D crack path and SIF predictions, and it is used to estimate the number of delay cycles associated with crack bifurcation. In the next sections, these two pieces of software are used to calculate the propagation behavior of kinked and bifurcated (branched) cracks.

2. Mixed-mode crack growth calculations

In FE mixed-mode crack growth calculations, three methods are generally used to compute the stress intensity factors along the (generally curved) crack path: the displacement correlation technique [11], the potential energy release rate computed by means of a modified crack-closure integral technique [12,13], and the J-integral computed by means of the equivalent domain integral (EDI) together with a mode decomposition scheme [14,15]. The EDI method replaces the J-integral along a contour by another one over a finite size domain, using the divergence theorem, which is more convenient for FE analysis.

Since Bittencourt et al. [16] showed that for sufficiently refined FE meshes all three methods predict essentially the same results, only the EDI method is considered in the calculations presented here. However, the other two methods also provide good results even for relatively coarse meshes.

The calculated Modes I and II SIF K_I and K_{II} are then used to obtain an equivalent SIF K_{eq}. The fatigue crack growth rate can then be computed from the equivalent stress intensity range ΔK_{eq} by a simple McEvily-type model [17]:

$$\frac{da}{dN} = A \cdot (\Delta K_{eq} - \Delta K_{th})^m \tag{1}$$

where ΔK_{th} is the threshold SIF and A and m are the conventional tensile crack growth rate parameters for the given material. An alternative Elber-type equation can be used based on the maximum equivalent stress intensity K_{eq} and on the crack opening value K_{op}, namely

$$\frac{da}{dN} = A \cdot (K_{eq} - K_{op})^m \tag{2}$$

Several models have been proposed to obtain K_{eq} from K_I and K_{II} (and K_{III}, when it is important). For example, Tanaka [18] obtained an equivalent stress intensity model based on the displacements behind the crack tip reaching a critical value, leading to

$$K_{eq} = \left[K_I^4 + 8 \cdot K_{II}^4 + \frac{8 \cdot K_{III}^4}{1 - \nu} \right]^{1/4} \tag{3}$$

where ν is Poisson's coefficient.

Another expression for K_{eq} can be derived for elastic loading under plane stress conditions, based on the relations between the potential energy release rate G and the SIF [19], leading to

$$K_{eq} = \sqrt{K_I^2 + K_{II}^2 + (1 + \nu) \cdot K_{III}^2} \tag{4}$$

Hussain et al. [20] used complex variable mapping functions to obtain G at a direction θ with respect to the crack propagation plane under Modes I and II combined loading. They assumed that crack extension occurs in a direction $\theta = \theta_0$ that maximizes G, leading to the maximum fracturing energy release rate (G_{max}) criterion. Thus, an equivalent SIF is obtained at $\theta = \theta_0$ that maximizes the expression

$$K_{eq} = \sqrt{\frac{4}{(3+\cos^2\theta)^2}\left(\frac{1-\theta/\pi}{1+\theta/\pi}\right)^{\theta/\pi}\left[(1+3\cos^2\theta)K_I^2 - 8\sin\theta\cos\theta\cdot K_I K_{II} + (9-5\cos^2\theta)K_{II}^2\right]} \tag{5}$$

The computed θ_0 values at each calculation step are used to obtain the crack incremental growth direction—and thus the fatigue crack path—in the linear-elastic regime.

Sih [21] proposed a criterion for mixed-mode loading based on the strain energy density S around the crack tip. It is assumed that the crack propagates in a direction $\theta = \theta_0'$ that minimizes S. The associated equivalent SIF is then calculated at $\theta = \theta_0'$ that minimizes the expression

$$K_{eq}^2 = \frac{1}{4(1-2\nu)}\Big\{(3-4\nu-\cos\theta)(1+\cos\theta)\cdot K_I^2 + 2\sin\theta\cdot[\cos\theta-1+2\nu]\cdot K_I K_{II} + [4(1-\nu)(1-\cos\theta)+(1+\cos\theta)(3\cos\theta-1)]\cdot K_{II}^2 + 4K_{III}^2\Big\} \tag{6}$$

Erdogan and Sih [22] proposed the maximum circumferential stress ($\sigma_{\theta\max}$) criterion, which considers that crack growth should occur in the direction that maximizes the circumferential stress in the region close to the crack tip. They considered the stresses at the crack tip under combined Modes I and II loading, given by summing up the stress fields generated by each mode:

$$\sigma_r = \frac{1}{\sqrt{2\pi r}}\left\{\frac{1}{4}\left(5\cos\frac{\theta}{2}-\cos\frac{3\theta}{2}\right)\cdot K_I - \frac{1}{4}\left(5\sin\frac{\theta}{2}-3\sin\frac{3\theta}{2}\right)\cdot K_{II}\right\} \tag{7}$$

$$\sigma_\theta = \frac{1}{\sqrt{2\pi r}}\left\{\frac{1}{4}\left(3\cos\frac{\theta}{2}+\cos\frac{3\theta}{2}\right)\cdot K_I - \frac{3}{4}\left(\sin\frac{\theta}{2}+\sin\frac{3\theta}{2}\right)\cdot K_{II}\right\} \tag{8}$$

$$\tau_{r\theta} = \frac{1}{\sqrt{2\pi r}}\left\{\frac{1}{4}\left(\sin\frac{\theta}{2}+\sin\frac{3\theta}{2}\right)\cdot K_I + \frac{1}{4}\left(\cos\frac{\theta}{2}+3\cos\frac{3\theta}{2}\right)\cdot K_{II}\right\} = -\frac{2}{3}\frac{\partial\sigma_\theta}{\partial\theta} \tag{9}$$

where σ_r is the normal stress component in the radial direction, σ_θ is the normal stress component in the tangential direction and $\tau_{r\theta}$ is the shear stress component. These expressions are valid both for plane stress and plane strain. The maximum circumferential stress criterion assumes that crack growth begins on a plane perpendicular to the direction in which σ_θ is maximum. The maximum value of σ_θ is obtained when $\partial\sigma_\theta/\partial\theta$ is zero, which is equivalent to equating $\tau_{r\theta} = 0$, according to Eq. (9). The equation $\tau_{r\theta} = 0$ has a trivial solution $\theta = \pm\pi$ (for $\cos(\theta/2) = 0$), and a non-trivial solution $\theta = \theta_0''$ given by

$$\theta_0'' = 2\arctan\left(\frac{1}{4}\frac{K_I}{K_{II}} \pm \frac{1}{4}\sqrt{\left(\frac{K_I}{K_{II}}\right)^2 + 8}\right) \tag{10}$$

where the sign of θ_0'' is the opposite of the sign of K_{II}. According to the $\sigma_{\theta\max}$ criterion, the equivalent SIF is calculated at the value $\theta = \theta_0''$, which maximizes the expression

$$K_{eq} = \frac{1}{4}\left(3\cos\frac{\theta}{2}+\cos\frac{3\theta}{2}\right)\cdot K_I - \frac{3}{4}\left(\sin\frac{\theta}{2}+\sin\frac{3\theta}{2}\right)\cdot K_{II} \tag{11}$$

Several other criteria have been proposed in the literature, such as the ones by Nuismer, Amestoy et al., Richard, Schöllmann et al., and Pook, as presented in [23]. A few of these criteria even predict the warping angle of a 3-D crack subject to Mode III loading. A comprehensive review of the proposed equivalent SIF and propagation angle expressions can be found in [23].

All presented models have notable differences if the amount of Mode II loading is significant. For instance, under pure Mode II loading, the propagation angle θ is $\pm70.5°$, $\pm75°$ and $\pm82°$ according to the $\sigma_{\theta\max}$, $G_{\max}$ and $S_{\min}$ models, respectively, leading to K_{eq} values of approximately $1.15\cdot K_{II}$, $1.60\cdot K_{II}$ and $1.05\cdot K_{II}$ (assuming $\nu = 0.3$). In addition, Tanaka's model results in this case in $K_{eq} = 1.68\cdot K_{II}$, while

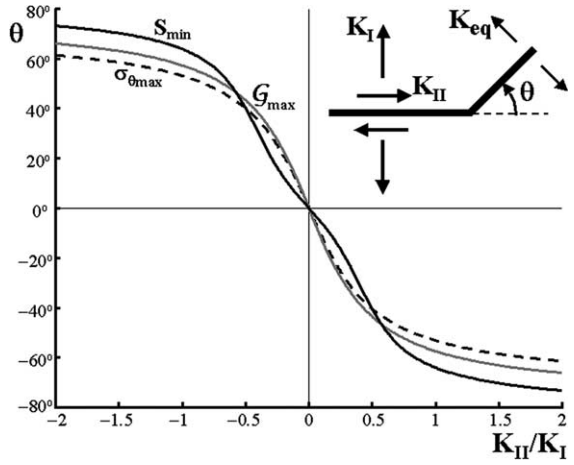

Fig. 2. Crack propagation direction θ as a function of the K_{II}/K_I ratio according to the $\sigma_{\theta\max}$, $G_{\max}$ and $S_{\min}$ models.

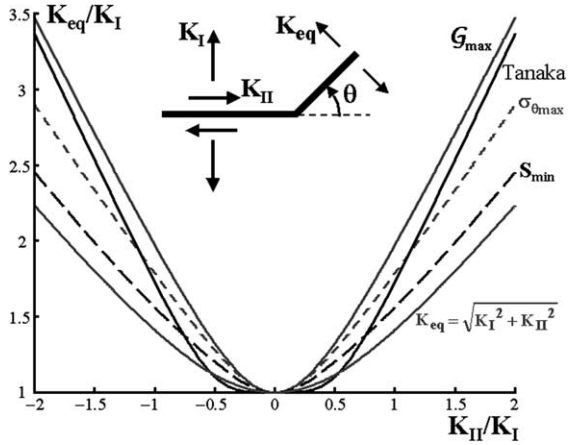

Fig. 3. Equivalent SIF K_{eq} as a function of the K_{II}/K_I ratio according to several models.

Eq. (4) furnishes $K_{eq} = K_{II}$. The values of θ and K_{eq} obtained from each model are plotted in Figs. 2 and 3 as a function of the K_{II}/K_I ratio.

The differences among the studied models might be significant for mixed-mode fracture predictions, however they turn out to be negligible for fatigue crack propagation calculations. In fact, since all above models predict crack path deviation ($\theta \neq 0$) under any K_{II} different than zero (see Fig. 2), they imply that fatigue cracks will always attempt to propagate in pure Mode I, minimizing the amount of Mode II loading, curving their paths if necessary to avoid rubbing their faces. As soon as the crack path is curved to follow pure Mode I, all models agree that K_{eq} is equal to K_I. Therefore, not only the crack path but also the associated SIF values calculated by any of the above criteria are essentially the same. This has been verified by Bittencourt et al. [16], who concluded from FE simulations that these criteria provide basically the same numerical results. Since the maximum circumferential stress criterion is the simplest, even presenting a closed form solution, it is the one adopted in the present work.

3. Crack kinking calculations

In this section, the Modes I and II SIF k_1 and k_2 are evaluated for cracks of length a with a small kink of length b_0 at an angle θ, see Fig. 4(a). According to [24,25], if b_0 is much smaller than all other crack dimensions, then k_1 and k_2 can be calculated from the Modes I and II SIF K_I and K_{II} of the straight crack (without the kink) using the approximate expressions:

$$k_1 = \frac{1}{4}\left(3\cos\frac{\theta}{2} + \cos\frac{3\theta}{2}\right)\cdot K_I - \frac{3}{4}\left(\sin\frac{\theta}{2} + \sin\frac{3\theta}{2}\right)\cdot K_{II} \tag{12}$$

$$k_2 = \frac{1}{4}\left(\sin\frac{\theta}{2} + \sin\frac{3\theta}{2}\right)\cdot K_I + \frac{1}{4}\left(\cos\frac{\theta}{2} + 3\cos\frac{3\theta}{2}\right)\cdot K_{II} \tag{13}$$

As discussed in [26], the exact analytical solution for k_1 and k_2 rests on the works in [27,28]. However, for all studied cases in this work, it is found that the average error resulting from the above approximate expressions is 1%, within the error tolerance of the FE calculations. It is interesting to note from Eqs. (12) and (13) that the stresses at the tip of a straight crack under combined Modes I and II may be related with the above solution by

$$\sigma_\theta = \frac{k_1}{\sqrt{2\pi r}} \quad \text{and} \quad \tau_{r\theta} = \frac{k_2}{\sqrt{2\pi r}} \Rightarrow k_2 = -\frac{2}{3}\frac{\partial k_1}{\partial \theta} \tag{14}$$

where the above relation between k_2 and k_1 can be obtained differentiating Eq. (12) and comparing it with (13), or from an analogy with Eq. (9).

Eqs. (12)–(14) are only valid for very small b_0/a ratios. On the other hand, when b_0/a is greater than 0.5, k_1 and k_2 are a weak function of b_0/a (being independent as b_0/a approaches infinity) for both kinked and symmetrically bifurcated cracks. This agrees with the fact that the solutions for kinked cracks with $b_0/a \gg 0.5$ approach those for an inclined crack:

$$k_1 = (\cos^2\theta)\cdot K_I - (\cos\theta\cdot\sin\theta)\cdot K_{II} \tag{15}$$

$$k_2 = (\cos\theta\cdot\sin\theta)\cdot K_I + (\cos^2\theta)\cdot K_{II} \tag{16}$$

To validate the Quebra2D program, the Modes I and II SIF k_1 and k_2 of an infinitesimally kinked crack ($b_0/a \to 0$ in Fig. 4(a)) are obtained and compared to the approximate solutions

$$k_1 = \frac{1}{4}\left(3\cos\frac{\theta}{2} + \cos\frac{3\theta}{2}\right)\cdot K_I \tag{17}$$

$$k_2 = \frac{1}{4}\left(\sin\frac{\theta}{2} + \sin\frac{3\theta}{2}\right)\cdot K_I \tag{18}$$

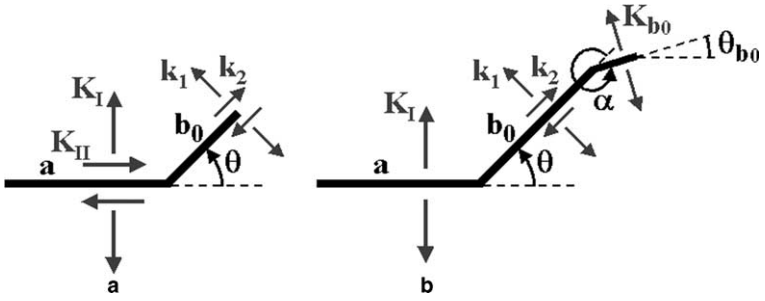

Fig. 4. Schematic representation of a kinked crack before propagation (a) and at the onset of propagation (b).

where K_I is the Mode I SIF of the straight crack without the kink (here K_{II} of the straight crack is assumed to be zero).

In order to numerically reproduce Eqs. (17) and (18), very small b_0/a ratios must be considered. Kitagawa et al. [29] performed numerical analyses using $b_0/a = 0.1$, however this ratio was not small enough to converge to the infinitesimal kink solution. In this work, a standard C(T) specimen is FE modeled with width $w = 32.0$ mm, crack length $a = 14.9$ mm, and a very small kink with length $b_0 = 10$ μm. The ratio $b_0/a = 10$ μm/14.9 mm $= 6.7 \times 10^{-4} \ll 0.1$ of this small kink is found appropriate to validate the infinitesimal kink assumption, through a convergence analysis on the calculated SIF. Note that this 10 μm choice is not related to the material or the grain size, since no micromechanisms are considered in the analysis, just the macroscopic behavior through the ratio b_0/a.

An efficient meshing algorithm is fundamental to avoid elements with poor aspect ratio when FE modeling this kink, since the ratio between the size scale of the larger and smaller elements is above 1000 in this case. To accomplish that, Quebra2D uses an innovative algorithm incorporating a quadtree procedure to develop local guidelines to generate elements with the best possible shape. The internal nodes are generated simultaneously with the elements, using the quadtree procedure only as a node-spacing function. This approach tends to give a better control over the generated mesh quality and to decrease the amount of heuristic cleaning-up procedures. Moreover, it specifically handles discontinuities in the domain or boundary of the model. Finally, to enhance the quality of the shape of the mesh element, an a posteriori local mesh improvement procedure is used [30].

It must be noted, however, that linear-elastic FE calculations can only lead to accurate solutions if the lengths of the crack branches b and c are significantly larger than the size scale of both the microstructure and the near-tip plastic (or process) zone. Microstructural effects are an important factor to determine the bifurcation event as well as the bifurcation angle and branch lengths. But as the crack branches grow further, the FE method can give a reasonable estimate of their behavior, in special for small process zones. In addition, the growth of branched cracks is typically transgranular, as verified from optical microscope observations performed by Shi et al. [31], which is one of the requirements to allow for the simulation of fatigue behavior in isotropic linear-elastic regime.

Fig. 5 shows a comparison between the analytical approximations and the FE-predicted k_1 and k_2 (normalized by the straight crack SIF K_I) for several kink angles θ, showing a very good agreement. The equivalent SIF K_{b0}, which is the crack rate controlling parameter, is then calculated based on the $\sigma_{\theta\max}$ criterion from Eq. (11), using $K_I \equiv k_1$ and $K_{II} \equiv k_2$. This K_{b0} can also be interpreted as the Mode I SIF of the kinked

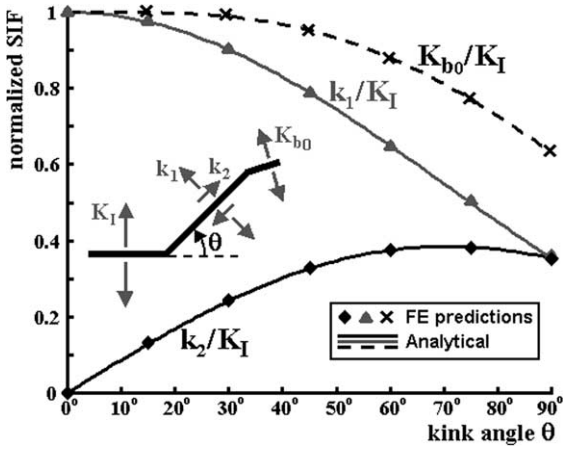

Fig. 5. Validation of the Quebra2D software for a kinked crack.

crack immediately after it starts propagating, soon after the expected sharp deflection is developed, see Fig. 5. Note that K_{b0} is only significantly smaller than the straight crack K_I (e.g. beyond 5%) for kink angles larger than 45°. Therefore, crack kinking is not a significant cause of retardation for kink angles smaller than 45°.

The equivalent SIF K_{b0} at the onset of the propagation can be calculated using the $\sigma_{\theta\max}$ criterion through Eqs. (10)–(13), however its expression is quite lengthy, see Eq. (19), where sign(x) is the sign function returning either 1, 0 or −1. Alternatively, a simple and practical function of θ (in degrees) can be successfully fitted to the calculated data within less than 1%, see Eq. (20).

$$\frac{K_{b0}}{K_I} = \frac{1}{16}\left(3\cos\frac{\theta_0''}{2}+\cos\frac{3\theta_0''}{2}\right)\left(3\cos\frac{\theta}{2}+\cos\frac{3\theta}{2}\right) - \frac{3}{16}\left(\sin\frac{\theta_0''}{2}+\sin\frac{3\theta_0''}{2}\right)\left(\sin\frac{\theta}{2}+\sin\frac{3\theta}{2}\right)$$
$$\theta_0'' = 2\arctan\left[\frac{1}{4}\cdot\frac{3\cos\theta/2+\cos 3\theta/2}{\sin\theta/2+\sin 3\theta/2} - \frac{1}{4}\cdot\operatorname{sign}\left(\sin\frac{\theta}{2}+\sin\frac{3\theta}{2}\right)\cdot\sqrt{\left(\frac{3\cos\theta/2+\cos 3\theta/2}{\sin\theta/2+\sin 3\theta/2}\right)^2+8}\right] \tag{19}$$

$$\frac{K_{b_0}}{K_I} = \begin{cases} 1, & \text{if } \theta \leqslant 10^\circ \\ 1 - 0.37\cdot\left(\dfrac{\theta-10^\circ}{80^\circ}\right)^{2.4}, & \text{if } \theta > 10^\circ \end{cases} \tag{20}$$

The initial propagation angle θ_{b0}, defined in Fig. 4(b), can also be calculated using the $\sigma_{\theta\max}$ criterion and fitted within less than 1% by the function:

$$\theta_{b_0} = \begin{cases} 0^\circ, & \text{if } \theta \leqslant 10^\circ \\ 37^\circ\cdot\left(\dfrac{\theta-10^\circ}{80^\circ}\right)^{1.7}, & \text{if } \theta > 10^\circ \end{cases} \tag{21}$$

In the next section, FE calculations are used to study the propagation behavior of kinked cracks, evaluating the crack retardation behavior and associated process zone size.

4. Propagation of kinked cracks

FE crack propagation simulations are performed to evaluate the retardation behavior of kinked cracks with angles θ equal to 15°, 30°, 45°, 60°, 75° and 90°. The crack parameter b is varied from its initial size b_0 to a final one b_f (measured along the crack path), where b_f is defined at the point beyond which the retardation effect ends, see Fig. 6. More specifically, the criterion to define b_f is to find the value of b beyond which the SIF of the bifurcated branch is equal to the original SIF within 1%. The ratios b_f/b_0 are calculated

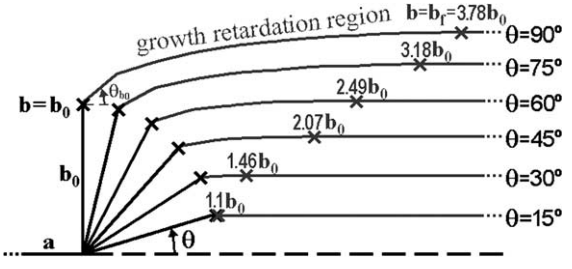

Fig. 6. Calculated crack paths for several kink angles.

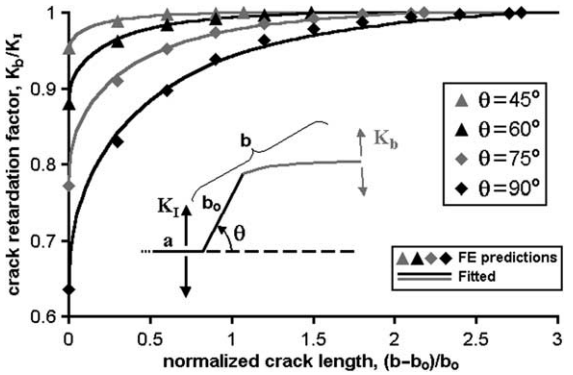

Fig. 7. Fitted and FE-calculated values of the equivalent SIF K_b along the crack path as a function of b.

as 1.1, 1.46, 2.07, 2.49, 3.18 and 3.78, respectively, for each of the kink angles considered in the simulations. These ratios are then fitted within 5% by the function of θ (in degrees):

$$\frac{b_f}{b_0} = \begin{cases} 1, & \text{if } \theta \leqslant 10^\circ \\ 1 + 2.8 \cdot \left(\dfrac{\theta - 10^\circ}{80^\circ}\right)^{1.3}, & \text{if } \theta > 10^\circ \end{cases} \tag{22}$$

The equivalent SIF K_b is then numerically calculated as a function of the crack length parameter b along the retardation region $b_0 \leqslant b \leqslant b_f$. An equation is then fitted within 2% to describe K_b as a function of K_I, K_{b0}, b, b_0 and b_f (see Fig. 7), resulting in

$$K_b = K_{b_0} + (K_I - K_{b_0}) \cdot \left[\operatorname{atan}\left(3\frac{b - b_0}{b_f - b_0}\right) \Big/ 1.25\right]^{0.4} \tag{23}$$

where atan is the arc-tangent function (in radians). Note that beyond the process zone, where $b > b_f$, K_b is equal to the straight crack K_I.

It can be concluded that crack kinking can reduce K_I by up to 37% if $\theta = 90^\circ$. However, the process zone size ahead of the crack tip, estimated by the difference $(b_f - b_0)$, is always relatively small (at most $2.8 \cdot b_0$ for $\theta = 90^\circ$).

Finally, substituting Eqs. (20) and (22) into (23), a single expression is obtained to model the retardation factor K_b/K_I of kinked cracks within 2%, valid for $b_0 \leqslant b \leqslant b_f$:

$$\frac{K_b}{K_I} = 1 - 0.37 \cdot \phi^{2.4}\left\{1 - \left[\operatorname{atan}\left(3 \cdot \frac{b/b_0 - 1}{2.8 \cdot \phi^{1.3}}\right) \Big/ 1.25\right]^{0.4}\right\} \tag{24}$$

where $\phi \equiv (\theta - 10^\circ)/80^\circ$ if $\theta > 10^\circ$, otherwise $\phi \equiv 0$. This expression can be readily used to predict the retardation behavior and number of delay cycles associated with crack kinking. In the next section, the present analysis is extended to bifurcated cracks.

5. Crack bifurcation predictions

In this section, the Modes I and II SIF are evaluated for cracks of length a with a small bifurcation of branch lengths b_0 and c_0 ($b_0 \geqslant c_0$) forming an angle 2θ, see Fig. 8(a). The calculations were performed on a standard C(T) specimen, FE modeled using Quebra2D assuming width $w = 32.0$ mm, crack length

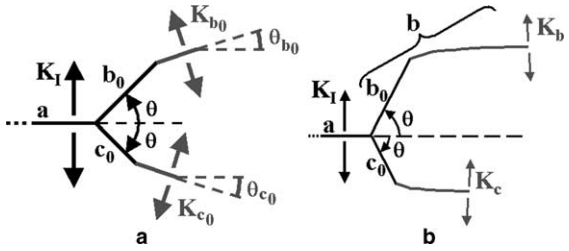

Fig. 8. Schematic representation of a branched crack at the onset of propagation (a) and during propagation (b).

$a = 14.9$ mm, and bifurcations with initial crack branch lengths $b_0 = 10$ μm and $c_0 = 5$, 7, 8, 9, 9.5 and 10 μm. The Modes I and II SIF k_1 and k_2 of each crack branch are obtained considering bifurcation angles 2θ between 15° and 168°. Note that typical overload-induced bifurcated cracks can have initial branch lengths between 10 and 100 μm, with 2θ varying between 30°, e.g. for very brittle materials such as glass, and 180°, e.g. in the vicinity of the interface of a bi-material composite, when a crack propagates from the weak to the strong material [32]. However, the studied $15° < 2\theta < 168°$ covers the range of most practical branched fatigue cracks in structural metallic alloys.

Fig. 9 shows the FE results for the SIF k_1 and k_2 (normalized by the Mode I SIF K_I of the straight crack) of symmetrically bifurcated cracks (which have $b_0 = c_0$). Note that k_2 vanishes for a bifurcation angle $2\theta = \theta^* = 53°$. The bifurcation angle $2\theta^*$ for which k_2 vanishes on a symmetrically branched crack is an important parameter, because it is associated with a self-similar propagation of the crack branches. Since k_2 is equal to zero, no crack path deflection will occur in this case, thus both their branches will continue propagating at an angle $\theta^* = \pm 26.5°$ with respect to the horizontal. Note however that the value of $2\theta^*$ is a function of the ratio b_0/a. For $b_0/a < 0.001$, $2\theta^*$ tends to approximately 53°, but for $b_0/a = 0.025$ the value of $2\theta^*$ drops to 36° [24] and for $b_0/a = 0.1$ it has been predicted that $2\theta^* = 32°$ [33]. Therefore, the infinitesimal kink solution shown in Fig. 9 can only be numerically reproduced using very refined FE calculations with b_0/a ratios much smaller than 0.1 or 0.025, such as the value considered in this work, $b_0/a = 10\ \mu\text{m}/14.9\ \text{mm} = 6.7 \times 10^{-4}$.

The FE-obtained k_1 and k_2 are now used to compute, using Eq. (11), an equivalent SIF K_{b0} of both branches that will characterize the propagation behavior immediately after the bifurcation event. Note from Fig. 9 that K_{b0}/K_I is approximately constant for symmetrically bifurcated cracks with

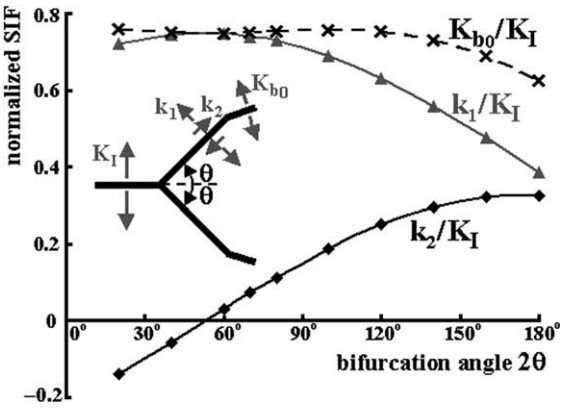

Fig. 9. Normalized stress intensity factors for symmetrically bifurcated cracks.

$2\theta < 140°$, estimated equal to 0.75 within 3%. But special care must be taken when calculating the SIF of bifurcated cracks with 2θ approaching 180°. In this case, the effective SIF increases considerably at the very beginning of the propagation. For instance, a symmetrically bifurcated crack with $2\theta = 160°$ has K_{b0}/K_I equal to 0.688 for both branches (as suggested in Fig. 9), however after a brief propagation of less than $0.1 \cdot b_0$ this value jumps to 0.751. Therefore, the decrease in K_{b0}/K_I for $2\theta > 140°$ shown in Fig. 9 is only valid at the onset of propagation, almost immediately increasing to approximately 0.75 after that. It is concluded from further simulations that K_{b0}/K_I can be estimated as 0.75 within 3% for all symmetrically bifurcated cracks with $40° \leqslant 2\theta \leqslant 168°$.

Figs. 10 and 11 show the FE results for the equivalent SIF K_{b0} and K_{c0} of the longer and shorter branches respectively (normalized by the Mode I SIF K_I of the straight crack), and the initial propagation angles, of both symmetrically and asymmetrically bifurcated cracks. Note once again the apparent decrease in K_{b0} for $2\theta > 140°$, an effect that disappears soon after the propagation starts. This high initial sensitivity can be explained by the small projected length of crack branches with 2θ approaching 180°. This projected

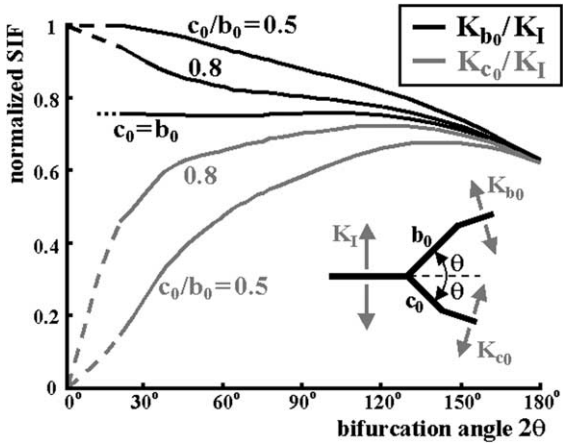

Fig. 10. Normalized equivalent stress intensity factors for symmetrically and asymmetrically bifurcated cracks.

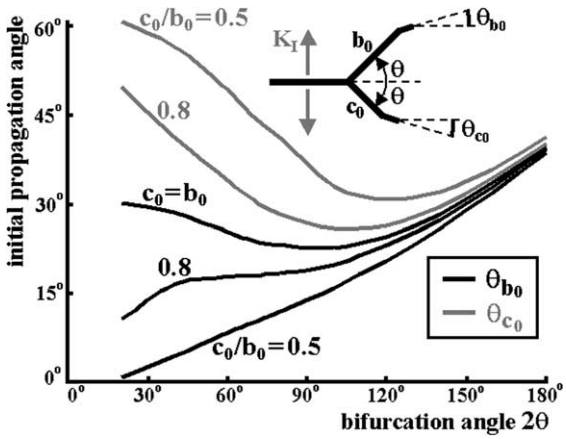

Fig. 11. Initial propagation angles for symmetrically and asymmetrically bifurcated cracks.

length is easily overcome even by a very small propagation step, significantly changing the crack geometry and SIF. For instance, a bifurcated crack with $2\theta = 170°$ has an initial propagation angle around 35° (Fig. 11), thus the crack branch b_0 has the same projected length as the one generated by a propagation step of only $b_0 \cdot \cos(0.5 \cdot 170°)/\cos(35°) \cong 0.11 \cdot b_0$.

Another interesting conclusion is that the initial propagation direction of the longer branch is always below 40° (with respect to the pre-overload growth direction), independently of the considered bifurcation angle 2θ, see Fig. 11. Therefore, for values of 2θ greater than 80°, a sharp deflection can be clearly noted in the beginning of the propagation. This deflection has been experimentally confirmed by Lankford and Davidson [1], who carried out overload fatigue crack tests on a 6061-T6 aluminum alloy in a scanning electron microscope using a special in situ servo-controlled hydraulic loading stage, obtaining growth retardation caused by crack bifurcation. They have found that the bifurcated crack would grow only a short distance in the same direction of the overload-induced bifurcation, before a sharp deflection in the crack path would occur, see Fig. 1.

This deflection causes a sudden increase in the Mode I SIF almost immediately after the propagation begins, resulting in a significantly smaller retardation effect if compared to simplistic predictions based on branched crack solutions that do not include the propagation phase. However, if the equivalent stress intensity ranges of both branches are below ΔK_{th}, then the entire crack arrests and therefore no sharp deflection has the chance to develop.

The FE-obtained results shown in Fig. 10 are used to fit empirical equations to the initial SIF K_{b0} and K_{c0} of the longer and shorter branches, resulting in

$$\frac{K_{b0}}{K_I} = 0.75 + (1 - \sin\theta) \cdot \left(1 - \frac{c_0}{b_0}\right) \tag{25}$$

$$\frac{K_{c0}}{K_I} = 0.75 - (1 - \sin\theta) \cdot \left(1 - \frac{c_0}{b_0}\right) \tag{26}$$

Eqs. (25) and (26) generate errors smaller than 2% for $40° \leqslant 2\theta \leqslant 168°$ and $0.7 \leqslant c_0/b_0 \leqslant 1.0$. Fig. 12 plots the FE results against the proposed equations, showing a good fit. In the next section, further FE analyses are conducted to evaluate the subsequent propagation behavior of these bifurcated cracks.

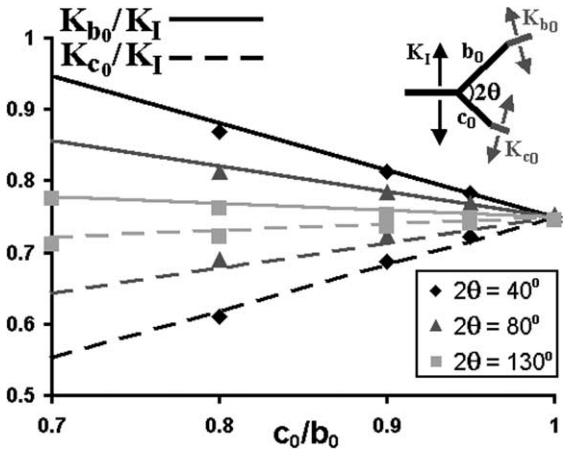

Fig. 12. Initial equivalent SIF of both branches of a bifurcated crack as a function of the asymmetry ratio c_0/b_0 and bifurcation angle 2θ.

6. Propagation of branched cracks

In this section, crack retardation equations are proposed to model the retardation effect along the path of the crack branches as a function of their ratio c_0/b_0, the bifurcation angle 2θ, and crack growth exponent m, considering no closure effects ($K_{op} = 0$). These equations are fitted to FE results obtained from the Quebra2D program using the same C(T) specimen described above. A fixed crack growth step of $\Delta b = 3$ μm (or 1 μm during the first propagation steps, corresponding respectively to 30% and 10% of the initial branch length) is considered for the propagation of the longer branch b. A sensitivity analysis using several crack propagation steps was performed to evaluate the convergence of the obtained crack path and stress intensity factors, validating the chosen calculation step. This growth step is calculated in the direction defined by the $\sigma_{\theta\max}$ criterion. Due to the differences in the crack growth rate, a growth step Δc smaller than Δb is expected for the shorter branch. This smaller step is obtained assuming a crack propagation law that models the first two growth phases,

$$\frac{da}{dN} = A \cdot (\Delta K - \Delta K_{th})^m \tag{27}$$

where A and m are material constants and ΔK_{th} is the propagation threshold. The effect of the R ratio can be considered if the constants A and m above are calibrated under the desired mean load condition. If ΔK_b and ΔK_c are respectively the stress intensity ranges of the longer and shorter branches, then the growth step Δc of the shorter branch c should be

$$\Delta c = \Delta b \cdot \left(\frac{\Delta K_c - \Delta K_{th}}{\Delta K_b - \Delta K_{th}}\right)^m \tag{28}$$

Interestingly, the ratio between the propagation rates of the two branches is independent of the material constant A. In this analysis, the exponent m is assumed to be 2.0, 3.0, and 4.0, which are representative for the range of the measured exponents for steels.

Once a (small) growth step Δb is chosen for the numerical propagation of the longer branch, the growth of the shorter branch Δc is readily obtained from Eq. (28). Both the crack path and the associated SIF along each branch are then obtained using the FE program.

Fig. 13 shows the contour plots of the normal stress component in the load direction axis and propagation results for a bifurcated crack with angle $2\theta = 150°$, obtained from the FE analysis for $c_0/b_0 = 0.91$, $m = 2$ and no closure. In this figure, the deformations are highly amplified to better visualize the crack path. Note that the crack path deviates from the original branch angles, deflecting from ±75° to approximately ±28°. In addition, the originally shorter branch arrests after propagating (only) about 29 μm, while the longer branch returns to the pre-overload growth direction and SIF (even though the subsequent crack growth plane may be offset from the pre-overload one, see Fig. 13).

Fig. 14 shows the crack paths obtained from the FE analyses of bifurcated cracks with $2\theta = 130°$ and $c_0/b_0 = \{0.5, 0.8, 0.95, 1\}$, considering $m = 2$ and no closure effects. The dashed lines show the theoretical propagation behavior of a perfectly symmetric bifurcation ($c_0/b_0 = 1$). In this case, the retardation effect would never end because both branches would propagate symmetrically without arresting. Clearly, such behavior is not observed in practice, since the slightest difference between b_0 and c_0 would be sufficient to induce an asymmetrical behavior.

The angles of the symmetrical dashed lines in Fig. 14 for small b_0/a ratios are found to be $\theta^* = \pm 26.5°$ with respect to the horizontal, where $2\theta^*$ has been previously defined as the bifurcation angle for which k_2 vanishes on a symmetrically branched crack. As the symmetrical branches grow following the ±26.5° directions, it is found that the ratio between the equivalent SIF and the SIF of a straight crack with same projected length is approximately constant and equal to 0.757, a value compatible with the 0.75 estimate for K_{b0}. Note that the directions ±26.5° are independent of 2θ, m, and the closure level, therefore symmetrical

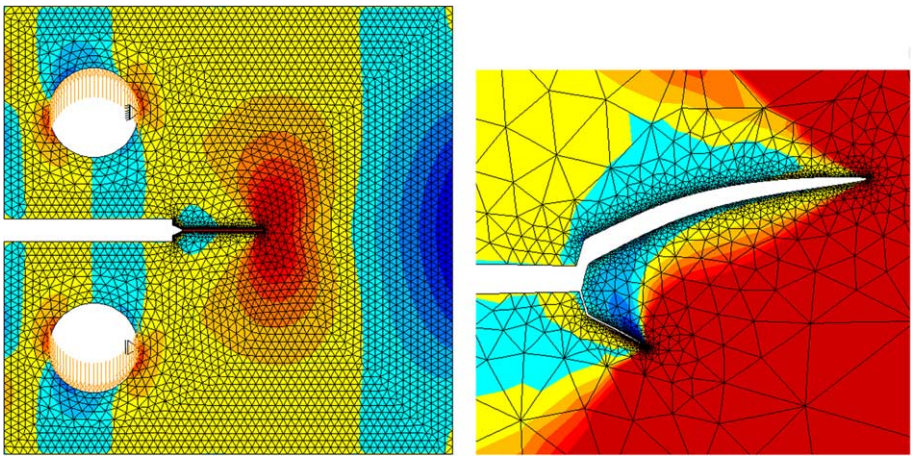

Fig. 13. Propagation simulation of a bifurcated crack on a C(T) specimen (left), and close-up view of the two original 11 μm and 10 μm branches with angle $2\theta = 150°$ (right).

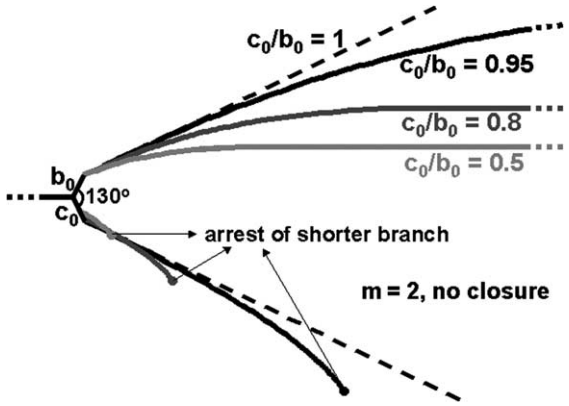

Fig. 14. Bifurcated crack paths for several c_0/b_0 ratios.

bifurcations with any initial angle 2θ would tend to the self-similar solution $2\theta^* = 53°$ as long as the ratio b/a of the propagating branches is sufficiently small. FE calculations also showed that the slopes of the dashed lines are gradually decreased as both branches grow, resulting in angles $\pm 18°$ in the vicinity of $b/a = 0.025$, $\pm 16°$ close to $b/a = 0.1$, and $\pm 15.3°$ for $b/a \gg 1$. This last result has been obtained from a FE analysis of a symmetrical bifurcation starting at the edge of a very large plate (therefore with $a = 0$ and $b/a \to \infty$).

Fig. 14 also shows that lower c_0/b_0 ratios result in premature arrest of the shorter crack branch, leading to smaller retardation zones. Also, the propagation path of the longer branch is usually restrained to the region within the dashed lines, while the shorter one is "pushed" outside that envelope due to shielding effects. This can also be implied from Fig. 11, which shows that the initial propagation angles of the shorter branch are always larger than the angles from the longer one.

The size of the retardation zone can be estimated from the ratio b_f/b_0, where b_f is the value of the length parameter b of the longer branch beyond which the retardation effect ends (in the same way that it was defined for kinked cracks). The ratio b_f/b_0 is then calculated through FE propagation simulations for all

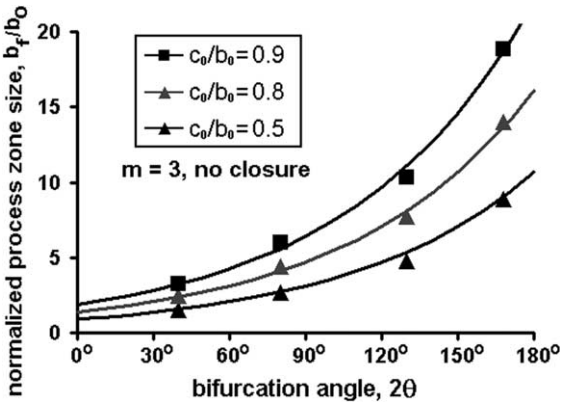

Fig. 15. Normalized process zone size as a function of the bifurcation angle and branch asymmetry c_0/b_0 ($m = 3$).

combinations of $c_0/b_0 = \{0.5, 0.8, 0.9, 0.95\}$, $2\theta = \{40°, 80°, 130°, 168°\}$ and $m = \{2, 3, 4\}$, and fitted by the proposed function:

$$\frac{b_f}{b_0} = \exp\left(\frac{2\theta - 30°}{56 + 17\cdot(m-2)^{2/3}}\right) \Big/ (1 - c_0/b_0)^{(12-m)/20} \tag{29}$$

Fig. 15 shows a comparison between the fitted and the FE-obtained data. Note that a greater symmetry between the branches (as c_0/b_0 approaches 1.0) results in a longer retardation zone, as expected from the delayed arrest of the shorter branch.

The FE-calculated equivalent SIF K_b and K_c of the longer and of the shorter branches are now evaluated along the obtained crack paths. Fig. 16(a) and (b) plot the crack retardation factors (defined as the ratios between K_b or K_c and the Mode I SIF K_I of a straight crack) for $2\theta = 130°$ and $m = 2$, as a function of the normalized length $(b - b_0)/b_0$ of the longer branch (measured along the propagation path). Because of the different crack branch lengths, the SIF at the longer one is much higher than that at the shorter branch. Assuming K_b and K_c to be the crack driving force, it can be seen from Fig. 16(a) and (b) that the longer branch reaches its minimum propagation rate right after the bifurcation occurs, returning to its pre-overload rate as the crack tip advances away from the influence of the shorter branch. As seen in the figure, the retardation behavior is misleadingly similar to closure-related effects, even though no closure is present in that case.

In addition, as the length difference between both branches increases, it is expected that the propagation rate of the shorter one is reduced until it arrests, after which the larger branch will dominate. Note that even small differences between the branch lengths, such as in the case $c_0/b_0 = 0.95$ shown in Fig. 16(a) and (b), are sufficient to cause subsequent arrest of the shorter branch, as verified in [34,35].

Fig. 17 shows the effect of the bifurcation angle 2θ on the retardation factor K_b/K_I for $c_0/b_0 = 0.9$ and $m = 3$. Note that the retardation effect lasts longer for larger bifurcation angles, not only because the associated Mode I SIF is smaller, but also because the shielding effect is weaker since both branch tips are further apart, delaying the arrest of the shorter one.

An empirical expression is here proposed to model the SIF K_b of the longer branch during the transition between K_{b0} (immediately after the bifurcation event) and the straight-crack K_I (after the end of the retardation effect), valid for $b_0 \leqslant b \leqslant b_f$ and $0.7 < c_0/b_0 < 1$:

$$K_b = K_{b_0} + (K_I - K_{b_0})\cdot\left[\operatorname{atan}\left(3\frac{b - b_0}{b_f - b_0}\right) \Big/ 1.25\right]^{2c_0/b_0} \tag{30}$$

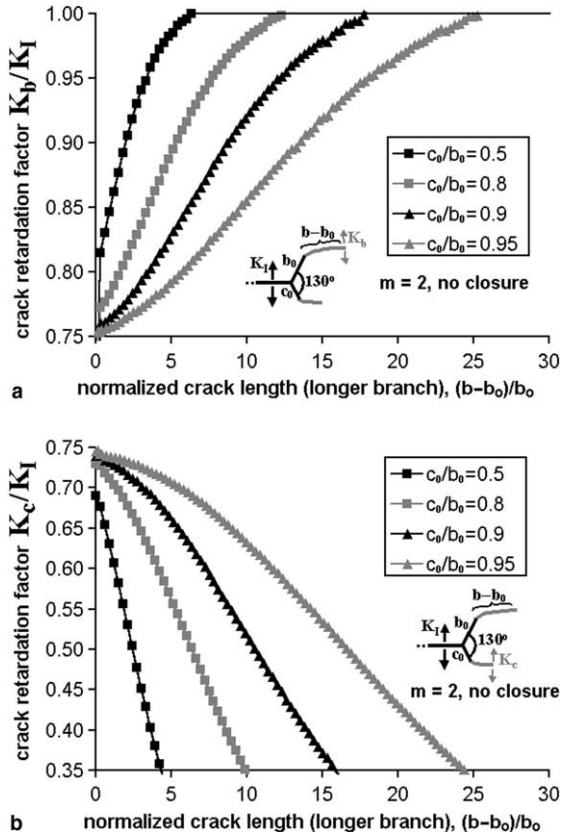

Fig. 16. Normalized equivalent SIF for (a) the longer branch and (b) the shorter branch of a bifurcated crack during its propagation ($2\theta = 130°$, $m = 2$).

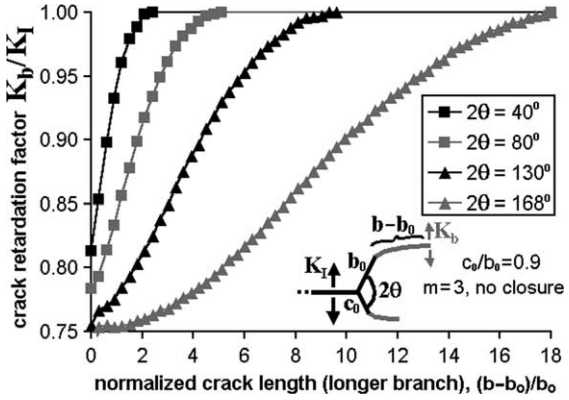

Fig. 17. Normalized SIF K_b/K_I of the longer branch during its propagation as a function of the normalized length $(b - b_0)/b_0$ for $c_0/b_0 = 0.9$, $m = 3$.

where K_{b0} and b_f are given in Eqs. (25) and (29). From these results, the predicted retardation behavior is plotted for several values of c_0/b_0, 2θ and m, as shown in Figs. 18–22.

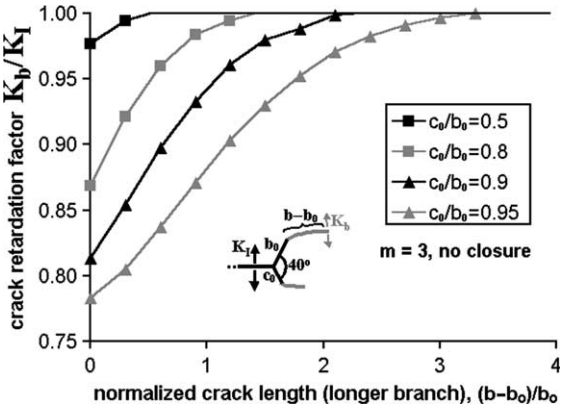

Fig. 18. Normalized SIF K_b/K_I of the longer branch during its propagation as a function of the normalized length $(b - b_0)/b_0$ for $2\theta = 40°$, $m = 3$.

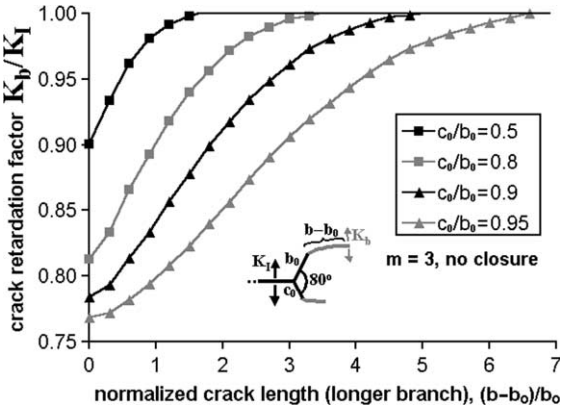

Fig. 19. Normalized SIF K_b/K_I of the longer branch during its propagation as a function of the normalized length $(b - b_0)/b_0$ for $2\theta = 80°$, $m = 3$.

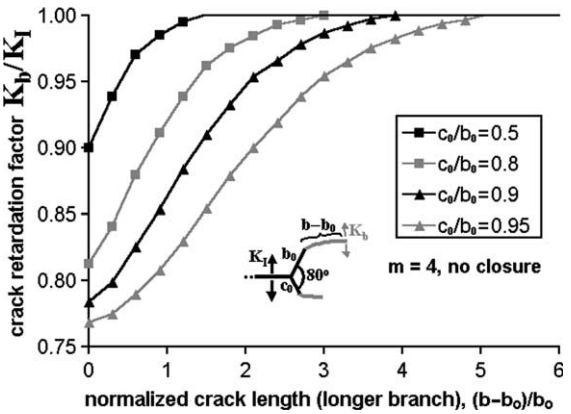

Fig. 20. Normalized SIF K_b/K_I of the longer branch during its propagation as a function of the normalized length $(b - b_0)/b_0$ for $2\theta = 80°$, $m = 4$.

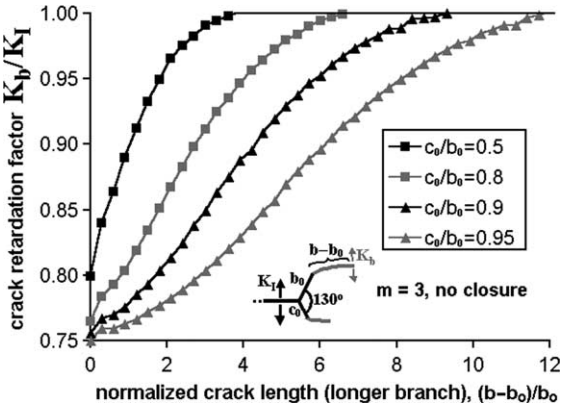

Fig. 21. Normalized SIF K_b/K_I of the longer branch during its propagation as a function of the normalized length $(b - b_0)/b_0$ for $2\theta = 130°$, $m = 3$.

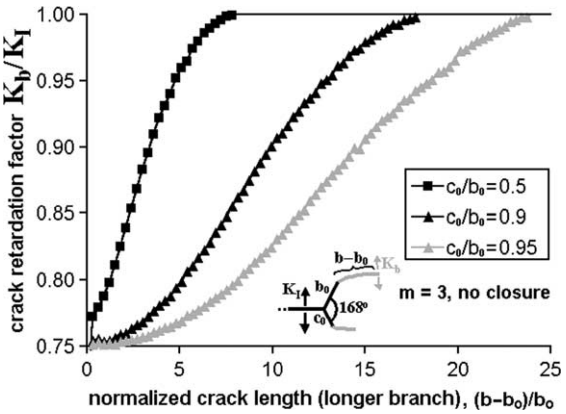

Fig. 22. Normalized SIF K_b/K_I of the longer branch during its propagation as a function of the normalized length $(b - b_0)/b_0$ for $2\theta = 168°$, $m = 3$.

Finally, it should be noted that all proposed equations are, at least in theory, applicable to any bifurcated crack in any specimen, provided that the crack branches are small if compared to the specimen geometry and that the propagation behavior of the material can be described using Eq. (27).

7. Experimental results

In this section, both qualitative and quantitative validations are performed on the presented methodology. A qualitative validation of the predicted bifurcated crack growth behavior is performed using 63 mm-wide, 10 mm-thick compact tension C(T) test specimens, made of SAE 1020 steel with yield strength $S_Y = 285$ MPa, ultimate strength $S_U = 491$ MPa, Young's modulus $E = 205$ GPa, and reduction in area RA = 54%, measured according to the ASTM E 8 M-99 standard. The analyzed weight percent composition of this steel is: C 0.19, Mn 0.46, Si 0.14, Ni 0.052, Cr 0.045, Mo 0.007, Cu 0.11, Nb 0.002, Ti 0.002. The tests are performed at frequencies between 20 and 30 Hz in a 250 kN computer-controlled servo-hydraulic testing machine. The crack length is measured following ASTM E 647-99 procedures.

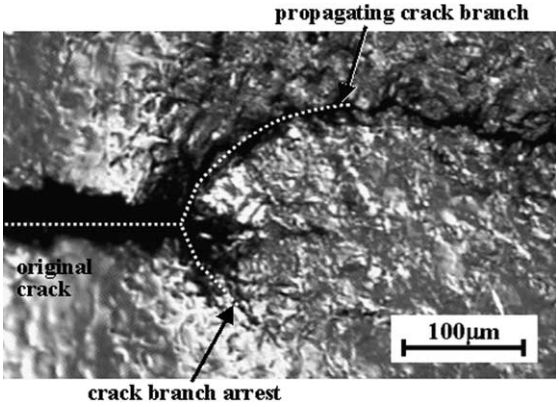

Fig. 23. Crack bifurcation experiments on 1020 steel.

Fig. 23 shows the measured paths of a branched crack induced by a 70% overload. As predicted, the shorter branch tends to arrest as the longer one continues to grow, returning to its original propagation direction. Note that the overload-induced bifurcation event caused large plastic zones, along which the branches extended. The main effects of these plastic zones would be crack closure, which would need to be combined with the bifurcation effects using an elastic–plastic approach. However, in all considered experiments, the loading ratio R was kept high enough to avoid closure-induced effects, therefore minimizing the effect of the plastic zone that always accompanies the crack tip. Beyond this overload plastic zone region, the zigzag pattern observed in the figure is probably caused by microstructural effects, however these zigzag kinks under 30° do not significantly influence the stress intensity factors, as indicated by Fig. 5. Despite the microstructurally induced zigzag pattern, the overall bifurcated crack propagation path is typically transgranular, showing a good match between the measured and the FE predicted crack paths. In addition, scanning electron micrographs of the specimen fracture surface show a through-the-thickness bifurcation front, see Fig. 24, validating the 2D approach adopted in the FE analysis.

The same crack growth behavior is observed on Eccentrically loaded Single Edge Crack Tension specimens ESE(T) made from an annealed SAE 4340 alloy steel with $S_Y = 377$ MPa, $S_U = 660$ MPa, $E = 205$ GPa, and RA = 52.7%, and with the analyzed weight percent composition: C 0.37, Mn 0.56, Si 0.14, Ni 1.53, Cr 0.64, Mo 0.18, S 0.04, P 0.035. The specimen dimensions are given in Fig. 25. The tests are performed under the same conditions used on the SAE 1020 specimens, with a baseline stress intensity range $\Delta K_I = 12.8$ MPa $\sqrt{\text{m}}$ and $R = 0.5$.

Fig. 26 shows the measured paths of a branched crack induced by a 50% overload when the crack length was $a = 25.55$ mm. In this case the original crack experienced kinking before the actual bifurcation event. However, the subsequent bifurcated crack propagation path showed good agreement with the linear elastic FE calculations. The zigzag pattern is also present at this branched propagation, however it does not significantly affect the SIF values. Scanning electron micrographs also confirm the through-the-thickness condition of the bifurcation front in all 4340 steel experiments.

Fig. 27 shows the retardation effect induced by the bifurcation, leading to approximately 12,600 delay cycles along a process zone of about 0.3 mm.

Fatigue crack opening loads are obtained in this work from the slope changes in the compliance $P \times \varepsilon$ (or in the load versus displacement, $P \times \delta$) curves of the test specimens. Fig. 28 shows opening load measurements versus back face strain ε for the SAE 4340 specimen, before and after the overload that caused the bifurcation. These curves are shifted in the figure for clarity, and their linear portion is subtracted using a highly sensitive linearity subtractor circuit connected to an analog computer that differentiated

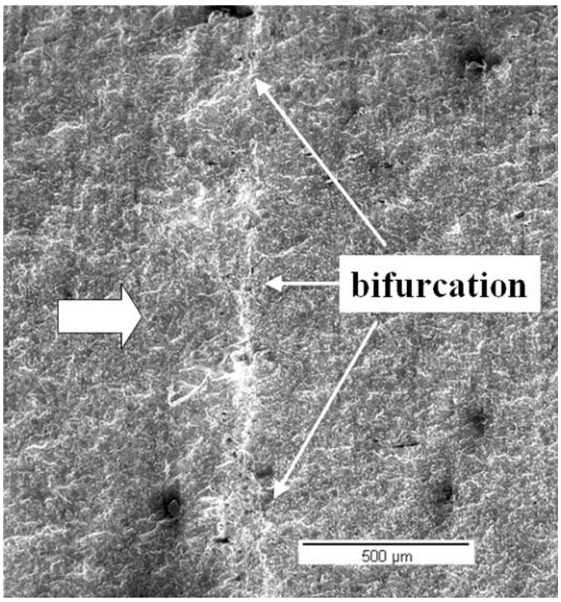

Fig. 24. Scanning electron micrograph of the 1020 steel specimen fracture surface, showing a through-the-thickness bifurcation front.

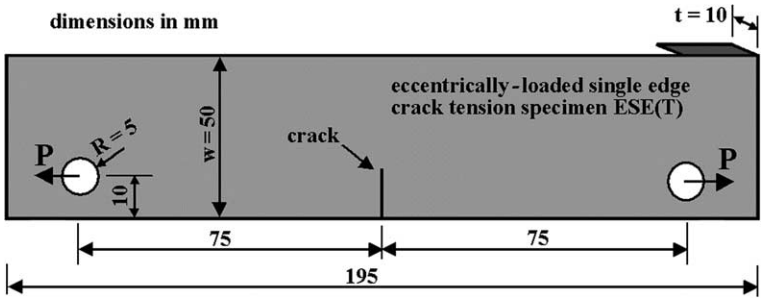

Fig. 25. Geometry of the tested 4340 steel ESE(T) specimen.

its output [36]. These instruments were specially designed and built to enhance the non-linear part of the $P \times \varepsilon$ signal. The back face strain ε is a more robust signal than the crack mouth opening displacement δ in the tests reported here, but both are used in all the measurements and presented identical results. The K_{op} measurement uncertainty of this experimental setup is small, and it can easily detect variations of only 1% in the opening loads. As seen in Fig. 28, the $R = 0.5$ level resulted in no closure effects neither before nor after the overload, because the opening load always remained below the minimum value of the applied load range ΔP. Therefore, it can be concluded that the measured retardation effect cannot be explained by crack closure. In fact, the bifurcation event even reduced the closure level by 25% due to the increased compliance caused by the crack branches. Clearly, retardation effects associated with a reduction in K_{op} would be incompatible with any retardation model based on crack closure. It is implied then that bifurcation is the dominant retardation mechanism.

The proposed retardation equations were implemented in a fatigue life assessment program named ViDa. This program is used to estimate the number of delay cycles associated with the experimentally obtained bifurcation on the 4340 steel ESE(T) specimen. The measured initial branch lengths are

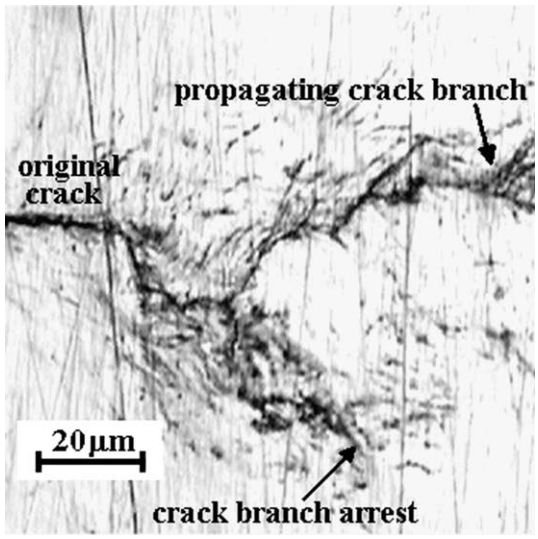

Fig. 26. Crack branching on an SAE 4340 ESE(T) specimen.

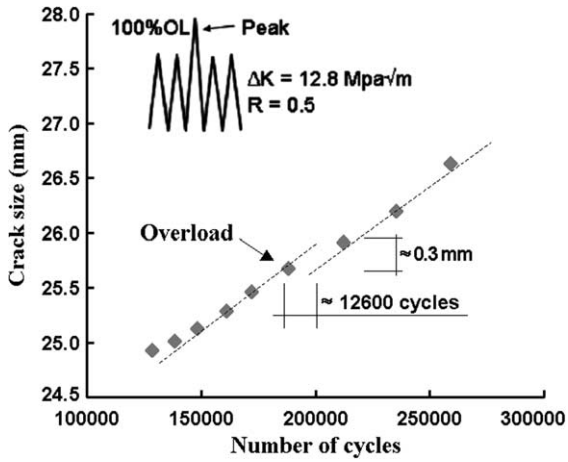

Fig. 27. Fatigue crack growth retardation after a 100% overload, $R = 0.5$ (SAE 4340).

approximately $b_0 = 20$ μm and $c_0 = 16$ μm, with a bifurcation angle $2\theta = 150°$. The fatigue crack growth in this material is modeled using Eq. (27) using $A = 9 \times 10^{-11}$ m/cycle and $m = 2.2$, and a propagation threshold $\Delta K_{th} = 3.8$ MPa $\sqrt{}$m, all measured under $R = 0.5$. Since no closure effects were present under such high load ratio, it can be concluded that 3.8 MPa $\sqrt{}$m is in fact the intrinsic threshold SIF of this material. From Eqs. (25) and (26), it is found that

$$\frac{K_{b0}}{K_I} = 0.75 + (1 - \sin 75°) \cdot \left(1 - \frac{16}{20}\right) \cong 0.757 \tag{31}$$

$$\frac{K_{c0}}{K_I} = 0.75 - (1 - \sin 75°) \cdot \left(1 - \frac{16}{20}\right) \cong 0.743 \tag{32}$$

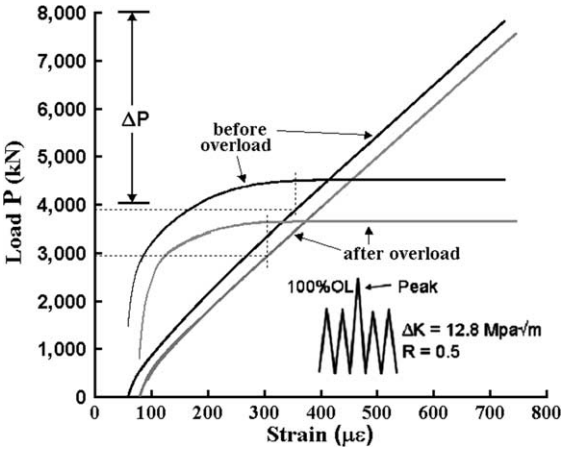

Fig. 28. Opening load measurements, including a linearity subtractor [36] to enhance the nonlinear part of the load versus back face strain ε (SAE 4340).

For the baseline stress intensity range $\Delta K_I = 12.8$ MPa $\sqrt{m}$, Eqs. (31) and (32) lead to $\Delta K_{b0} = 0.757 \cdot \Delta\varpi$ $K_I = 9.69$ and $\Delta K_{c0} = 0.743 \cdot \Delta K_I = 9.51$ MPa $\sqrt{m}$. Since both ranges are greater than $\Delta K_{th}(R = 0.5) =$ 3.8 MPa $\sqrt{m}$, both branches are expected to start propagating, as verified experimentally. Since the measured K_{op} was smaller than the minimum applied SIF (Fig. 28), no closure effects need to be considered, and the size of the process zone can be estimated from Eq. (29):

$$\frac{b_f}{b_0} = \exp\left(\frac{150^\circ - 30^\circ}{56 + 17 \cdot (2.2-2)^{2/3}}\right) \Big/ \left(1 - \frac{16}{20}\right)^{\left(\frac{12-2.2}{20}\right)} \cong 15.33 \tag{33}$$

which results in $b_f = 15.33 \times 20\ \mu m \cong 307\ \mu m$, matching very well the measured process zone size of 0.3 mm.

The number of cycles spent to grow the crack in the retardation region is then calculated by integrating the da/dN equation along the longer crack branch, from $b = b_0$ to $b = b_f$. Assuming that the longer branch path is approximately parallel to the original straight crack, then the number of delay cycles n_D can be estimated by integrating Eqs. (27)–(30):

$$\begin{aligned} n_D &= \int_{b_0}^{b_f} \frac{db}{A(\Delta K_b - \Delta K_{th})^m} - \int_{b_0}^{b_f} \frac{db}{A(\Delta K_I - \Delta K_{th})^m} \\ &= \int_{20}^{307} \frac{db \times 10^{-6}}{9 \times 10^{-11}\left\{5.89 + 3.11 \cdot \left[\operatorname{atan}\left(3\,\frac{b-20}{307-20}\right)/1.25\right]^{1.6}\right\}^{2.2}} - \int_{20}^{307} \frac{db \times 10^{-6}}{9 \times 10^{-11}(12.8-3.8)^{2.2}} \\ &= 37,361 - 25,337 = 12,024 \text{ cycles} \end{aligned} \tag{34}$$

which is very close to the measured 12,600 delay cycles. Therefore, both process zone size and number of delay cycles are reasonably well estimated from the proposed equations.

8. Conclusions

In this work, a specialized FE program was used to calculate the propagation path and associated stress intensity factors (SIF) of kinked and bifurcated cracks, which can cause crack retardation or even arrest. A

total of 52 crack propagation simulations were obtained from approximately 1250 FE calculation steps to fit empirical equations to the process zone size and crack retardation factor along the curved crack path. In particular, the bifurcation simulations included several combinations of bifurcation angles $2\theta = \{40°, 80°, 90°, 130°, 168°\}$, branch asymmetry ratios $c_0/b_0 = \{0.5, 0.7, 0.8, 0.9, 0.95, 1.0\}$, and crack growth exponents $m = \{2, 3, 4\}$.

It was found that crack kinking is not a significant cause of retardation for kink angles smaller than 45°, however it can reduce the SIF by up to 37% for angles approaching 90°. Crack bifurcation can also reduce the SIF to about 0.63 of its original value. However, soon after the branches start propagating, this value stabilizes at 0.75, as long as the branches are approximately symmetrical. It was also shown that very small differences between the lengths of the bifurcated branches are sufficient to cause the shorter one to eventually arrest as the longer branch returns to the pre-overload propagation conditions. The process zone size was found to be smaller for lower bifurcation angles and for branches with greater asymmetry, in both cases due to the increased shielding effects on the shorter branch. The retardation zone was reduced as well for materials with higher crack growth exponents, due to the increased difference between the crack growth rates of the longer and shorter branches.

Experiments were performed to validate the proposed equations. In the experiments, the separation between closure-induced and bifurcation-induced retardation was done using high R-ratio loading programs, guaranteeing closure-free conditions through compliance measurement tests. It was found that the proposed model predictions were able to both physically and quantitatively explain crack growth retardation as a result of crack kinking and branching, without the need to fit empirical constants.

The proposed equations, besides capturing all above described phenomena, can be readily used to predict the propagation behavior of branched and kinked cracks in an arbitrary structure, as long as the process zone is small compared to the other characteristic dimensions. These expressions were qualitatively and quantitatively validated through bifurcation experiments on 1020 and 4340 steel specimens. Careful inspection of the fracture surfaces using a scanning electron microscope revealed that all tests resulted in a uniform bifurcation front along the specimen thickness. The bifurcation front was approximately straight and through-the-thickness, validating the adopted FE hypotheses. Comparisons were made between the experiments and life assessment calculations obtained from a specialized fatigue design program. From these results, it was shown that crack bifurcation might provide an alternate mechanistic explanation for overload-induced crack retardation, in special to justify load interaction effects under high R ratios, where closure-free conditions may arise in the presence of dominantly plane-strain conditions and low overload ratios (typically up to 100%).

It must be pointed out, however, that the presented mixed-mode equations might have some limitations, because actual bifurcations can be of a size comparable to the scale of the local plasticity (e.g., of the plastic zone size) or microstructural features (e.g., of the grain size). Moreover, possible closure and environmental effects should be considered when comparing the bifurcation model predictions with measured crack growth rates [2]. A more detailed analysis could include micromechanisms leading to crack propagation considering, e.g., cleavage. The presented FE calculations assume linear-elastic, isotropic and homogeneous conditions that would not be applicable if micromechanisms were to be considered. Instead, the traditional fracture mechanics approach is taken, using stress intensity factor concepts to evaluate crack propagation on a macroscopic scale. It is a fact that near-threshold crack propagation rates can be as low as one atomic distance per cycle, in addition to the fact that all fatigue cracks cut through previously generated plastic zones. However, in all these cases, the macroscopic approach has proven to be successful. Assuming that the entire crack-front deflects uniformly, the specimen thickness itself may provide the size scale requirements for the validity of the presented equations, as the calculated SIF may be averaged considering the (several) grains present along the thickness, which validates the proposed approach. Otherwise, if the crack deflections vary significantly along the thickness, then further modeling including Mode III effects should be considered.

In summary, even though microstructure can be the cause for the observed bifurcations (which are not predicted beforehand using FE elements), the subsequent propagation can be calculated using a macroscopic approach as long as the bifurcation geometry is given as an input.

References

[1] Lankford J, Davidson DL. The effect of overloads upon fatigue crack tip opening displacement and crack tip opening/closing loads in aluminum alloys. Advances in fracture research, vol. 2. Pergamon Press; 1981. p. 899–906.
[2] Suresh S. Crack deflection: implications for the growth of long and short fatigue cracks. Metall Trans 1983;14a:2375–85.
[3] Kosec B, Kovacic G, Kosec L. Fatigue cracking of an aircraft wheel. Engng Failure Anal 2002;9:603–9.
[4] Suresh S. Micromechanisms of fatigue crack growth retardation following overloads. Engng Fract Mech 1983;18(3):577–93.
[5] Suresh S. Fatigue of materials. Cambridge: Cambridge University Press; 1998. 679p.
[6] Seelig T, Gross D. On the interaction and branching of fast running cracks—a numerical investigation. J Mech Phys Solids 1999;47:935–52.
[7] Karihaloo BL. On crack kinking and curving. Mech Mater 1982;1:189–201.
[8] Suresh S, Shih CF. Plastic near-tip fields for branched cracks. Int J Fract 1986;30:237–59.
[9] Miranda ACO, Meggiolaro MA, Castro JTP, Martha LF, Bittencourt TN. Fatigue crack propagation under complex loading in arbitrary 2D geometries. In: Braun AA, McKeighan PC, Lohr RD, editors. Applications of automation technology in fatigue and fracture testing and analysis, ASTM STP 1411, vol. 4, 2002. p. 120–46.
[10] Meggiolaro MA, Castro JTP. ViDa—danometro visual para automatizar o projeto à Fadiga sob carregamentos complexos. Brazil J Mech Sci 1998;20(4):666–85 [in Portuguese].
[11] Shih CF, de Lorenzi HG, German MD. Crack extension modeling with singular quadratic isoparametric elements. Int J Fract 1976;12:647–51.
[12] Raju IS. Calculation of strain-energy release rates with higher order and singular finite elements. Engng Fract Mech 1987;28:251–74.
[13] Rybicki EF, Kanninen MF. A finite element calculation of stress-intensity factors by a modified crack closure integral. Engng Fract Mech 1977;9:931–8.
[14] Dodds RH Jr, Vargas PM. Numerical evaluation of domain and contour integrals for nonlinear fracture mechanics. Report, Department of Civil Engineering, University of Illinois, Urbana-Champaign, 1988.
[15] Nikishkov GP, Atluri SN. Calculation of fracture mechanics parameters for an arbitrary three-dimensional crack by the equivalent domain integral method. Int J Numer Meth Engng 1987;24:1801–21.
[16] Bittencourt TN, Wawrzynek PA, Ingraffea AR, Sousa JLA. Quasi-automatic simulation of crack propagation for 2D LEFM problems. Engng Fract Mech 1996;55:321–34.
[17] McEvily AJ. Current aspects of fatigue. Metal Sci 1977;11:274–84.
[18] Tanaka K. Fatigue propagation from a crack inclined to the cyclic tensile axis. Engng Fract Mech 1974;6:493–507.
[19] Irwin GR. Analysis of stresses and strains near the end of a crack transversing a plate. Appl Mech J 1957;24:361–70.
[20] Hussain MA, Pu SU, Underwood J. Strain energy release rate for a crack under combined mode I and II. ASTM STP 560, 1974. p. 2–28
[21] Sih GC. Strain-energy–density factor applied to mixed mode crack problems. Int J Fract Mech 1974;10:305–21.
[22] Erdogan F, Sih GC. On the crack extension in plates under plane loading and transverse shear. J Basic Engng 1963;85:519–27.
[23] Richard HA. Theoretical crack path determination. In: International conference on fatigue crack paths, Parma, Italy, 2003.
[24] Bilby BA, Cardew GE, Howard IC. Stress intensity factors at the tips of kinked and forked cracks. In: Taplin DMR, editor. Fracture 1977, vol. 3. New York: Pergamon Press; 1977.
[25] Cotterell B, Rice JR. Slightly curved or kinked cracks. Int J Fract 1980;16:155–69.
[26] Melin S. Why do cracks avoid each other? Int J Fract 1983;23:37–45.
[27] Khrapkov AA. The first basic problem for a notch at the apex at an infinite wedge. Int J Fract 1970;7(4):373–82.
[28] Melin S. Accurate data for stress intensity factors at infinitesimal kinks. J Appl Mech 1994;61:467–70.
[29] Kitagawa H, Yuuki R, Ohira T. Crack-morphological aspects in fracture mechanics. Engng Fract Mech 1975;7:515–29.
[30] Miranda ACO, Meggiolaro MA, Castro JTP, Martha LF, Bittencourt TN. Fatigue life and crack path prediction in generic 2D structural components. Engng Fract Mech 2003;70:1259–79.
[31] Shi HJ, Niu LS, Mesmacque G, Wang ZG. Branched crack growth behavior of mixed-mode fatigue for an austenitic 304L steel. Int J Fatigue 2000;22:457–65.
[32] Pippan R, Flechsig K, Riemelmoser FO. Fatigue crack propagation behavior in the vicinity of an interface between materials with different yield stresses. Mater Sci Engng A 2000;283:225–33.
[33] Lo KK. Analysis of branched cracks. J Appl Mech 1978;45:797–802.

[34] Paxon TL, Lucas RA. An experimental investigation of the velocity characteristics of a mixed boundary fracture model. In: Sih GC, editor. Proceedings of the international conference on dynamic crack propagation. Leyden: Noordhoff Int. Publishing; 1973. p. 415–26.
[35] Pärletun LG. Determination of the growth of branched cracks by numerical methods. Engng Fract Mech 1979;11(2):343–58.
[36] Castro JTP. A circuit to measure crack closure. Exp Techniques 1993;17(2):23–5.